

Theoretical prediction and experimental evaluation of topological landscape and thermodynamic stability of a fluorinated zeolitic imidazolate framework

Arhangel'skis, Mihails; Katsenis, Athanassios D.; Novendra, Novendra; Akimbekov, Zamirbek; Gandrath, Dayaker; Marrett, Joseph M.; Ayoub, Ghada; Morris, Andrew J.; Farha, Omar K.; Friš, Tomislav; Navrotsky, Alexandra

DOI:

[10.1021/acs.chemmater.9b00994](https://doi.org/10.1021/acs.chemmater.9b00994)

Document Version

Peer reviewed version

Citation for published version (Harvard):

Arhangel'skis, M, Katsenis, AD, Novendra, N, Akimbekov, Z, Gandrath, D, Marrett, JM, Ayoub, G, Morris, AJ, Farha, OK, Friš, T & Navrotsky, A 2019, 'Theoretical prediction and experimental evaluation of topological landscape and thermodynamic stability of a fluorinated zeolitic imidazolate framework', *Chemistry of Materials*, vol. 31, no. 10, pp. 3777-3783. <https://doi.org/10.1021/acs.chemmater.9b00994>

[Link to publication on Research at Birmingham portal](#)

Publisher Rights Statement:

Checked for eligibility: 19/06/2019

This document is the Accepted Manuscript version of a Published Work that appeared in final form in *Chemistry of Materials*, copyright © American Chemical Society after peer review and technical editing by the publisher. To access the final edited and published work see: <https://doi.org/10.1021/acs.chemmater.9b00994>

General rights

Unless a licence is specified above, all rights (including copyright and moral rights) in this document are retained by the authors and/or the copyright holders. The express permission of the copyright holder must be obtained for any use of this material other than for purposes permitted by law.

- Users may freely distribute the URL that is used to identify this publication.
- Users may download and/or print one copy of the publication from the University of Birmingham research portal for the purpose of private study or non-commercial research.
- User may use extracts from the document in line with the concept of 'fair dealing' under the Copyright, Designs and Patents Act 1988 (?)
- Users may not further distribute the material nor use it for the purposes of commercial gain.

Where a licence is displayed above, please note the terms and conditions of the licence govern your use of this document.

When citing, please reference the published version.

Take down policy

While the University of Birmingham exercises care and attention in making items available there are rare occasions when an item has been uploaded in error or has been deemed to be commercially or otherwise sensitive.

If you believe that this is the case for this document, please contact UBIRA@lists.bham.ac.uk providing details and we will remove access to the work immediately and investigate.

Theoretical Prediction and Experimental Evaluation of Topological Landscape and Thermodynamic Stability of a Fluorinated Zeolitic Imidazolate Framework

Mihails Arhangel'skii,^a Athanassios D. Katsenist,^a Novendra Novendra,^b Zamirbek Akimbekov,^b Dayaker Gandrath,^a Joseph M. Marrett,^a Ghada Ayoub,^a Andrew J. Morris,^c Omar K. Farha,^d Tomislav Friščić,^{a,*} and Alexandra Navrotsky^{b,*}

^aDepartment of Chemistry, McGill University, Montreal, QC, H3A 0B8, Canada; ^bPeter A. Rock Thermochemistry Laboratory and NEAT ORU, University of California Davis, One Shields Avenue, Davis, CA 95616, USA; ^cSchool of Metallurgy and Materials, University of Birmingham, Edgbaston, Birmingham B15 2TT, UK; ^dDepartment of Chemistry and International Institute for Nanotechnology, Northwestern University, Evanston, IL 60208, USA

ABSTRACT: The prediction of topological preferences and polymorph stability remains a challenge for the design of metal-organic frameworks (MOFs) exhibiting a rich topological landscape, such as zeolitic imidazolate frameworks (ZIFs). Here, we have used mechanochemical screening and calorimetry to test the ability of dispersion-corrected periodic density functional theory (DFT) to accurately survey the topological landscape, as well as quantitatively evaluate polymorph stability, for a previously not synthesized ZIF composition. Theoretical calculations were used to obtain an energy ranking and evaluate energy differences for a set of hypothetical, topologically-distinct structures of a fluorine-substituted ZIF. Calculations were then experimentally validated *via* mechanochemical screening and calorimetry which confirmed two out of three theoretically anticipated topologies, including a fluorinated analogue of the popular ZIF-8, while revealing an excellent match between the measured and theoretically calculated energetic difference between them. The results, which speak strongly in favor of ability of dispersion-corrected periodic DFT to predict the topological landscape of new ZIFs, also reveal the ability to use peripheral substituents on the organic linker to modify the framework thermodynamic stability.

Introduction

The experimental and computational design of metal-organic frameworks (MOFs)¹⁻⁴ has focused largely on the assembly of nodes and linkers of controlled size and rigid geometry.⁵⁻¹⁰ While the influence of linker substituents on MOF properties has recently been explored,¹¹ theoretical studies of how the substituents affect the topological landscape and thermodynamic stability of MOFs are rare and generally not experimentally validated.¹²⁻¹⁵ Such studies are especially relevant for zeolitic imidazolate frameworks (ZIFs), azolate MOFs¹⁶ analogous to zeolites. Like zeolites, ZIFs readily form polymorphs, often with a rich topological landscape that depends strongly on the choice and positioning of linker substituents. For example, zinc 2-methylimidazolate Zn(MeIm)₂ forms a family of increasingly dense and stable frameworks with sodalite (SOD), katsenite (*kat*) and diamondoid (*dia*) topology. Zinc 2-ethylimidazolate Zn(EtIm)₂ yields ZIFs of zeolite rho (RHO), analcime (ANA) and quartz (*qtz*) topology,¹⁷⁻²⁰ while unsubstituted imidazolate yields at least 15 polymorphs.²¹ Periodic density functional theory (DFT) has been extensively used to model ZIF polymorphism^{12-15,22-25} and generally predict MOF structures and properties.^{26,27} Our recent theoretical and experimental study shows²⁰ that periodic DFT with semi-empirical dispersion correction (SEDC) can provide not only the correct energy rank-

ing of Zn(MeIm)₂ and Zn(EtIm)₂ polymorphs, but also a reasonable evaluation of energy differences between them. This opens a route to use dispersion-corrected DFT to survey topological preferences of novel ZIFs by evaluating relative stabilities of topologically different hypothetical structures.²⁸

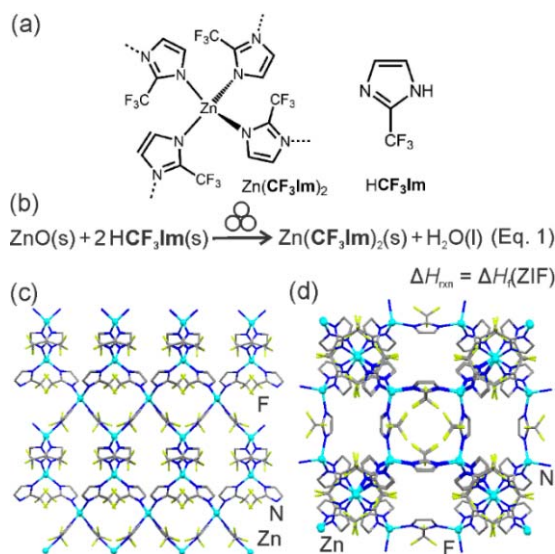


Figure 1. (a) Schematic representation of $\text{Zn}(\text{CF}_3\text{Im})_2$ and ligand 2-trifluoromethylimidazole (HCF_3Im); (b) synthesis of $\text{Zn}(\text{CF}_3\text{Im})_2$ from ZnO . Crystal structures of herein predicted and observed: (c) $qtz\text{-Zn}(\text{CF}_3\text{Im})_2$ and (d) $\text{SOD-Zn}(\text{CF}_3\text{Im})_2$.

We now test this approach by computationally screening and experimentally evaluating the topological preferences and stability for a previously not reported ZIF, zinc 2-trifluoromethylimidazolate ($\text{Zn}(\text{CF}_3\text{Im})_2$, Figure 1). We selected this model system because of the recent high interest in fluorinated MOF materials.²⁹⁻³⁷ Importantly, previous attempts to synthesize this material from solution were unsuccessful,³⁸ prompting us to explore mechanochemical methodologies known to offer access to otherwise inaccessible phases.³⁹

Computational and Experimental Methods

Computational Methods

The theoretically calculated putative structures for all $\text{Zn}(\text{CF}_3\text{Im})_2$ frameworks in Table 1 have been provided in the SI, in CIF format.

Computational screening, conducted prior to any experiments, was limited to putative $\text{Zn}(\text{CF}_3\text{Im})_2$ structures based on *dia*, *kat*, SOD, *qtz*, ANA, RHO, *zni* and *cag*-topologies that are often found in ZIFs. Structures were generated from ZIFs found in the Cambridge Structural Database (CSD),⁴⁰ by removing any guest molecules, inserting CF_3 groups into the 2-position of imidazolate linkers and replacing any 4- and 5-substituents with hydrogens. Some of the resulting structures exhibited short “head-to-head” or “tail-to-tail” F...F contacts, notably those with SOD-, *kat*-, ANA- and RHO-topologies in which substituents in a 4-ring are in close vicinity (Figures 2a,b), and *dia*- $\text{Zn}(\text{CF}_3\text{Im})_2$ where such contacts result from close packing. To minimize such contacts, neighboring $-\text{CF}_3$ groups were oriented into a “head-to-tail” arrangement (Figure 2c). This was readily done for *dia*- $\text{Zn}(\text{CF}_3\text{Im})_2$, but not for SOD-, *kat*-, ANA- and RHO-structures where the alignment of substituents is constrained by space group symmetry. For those topologies two structural models were evaluated, one considering full crystallographic symmetry of the parent CSD structure, and one with space group symmetry constraints removed to form a disordered $P1$ structure in which the relative orientations of $-\text{CF}_3$ groups could be independently manipulated.

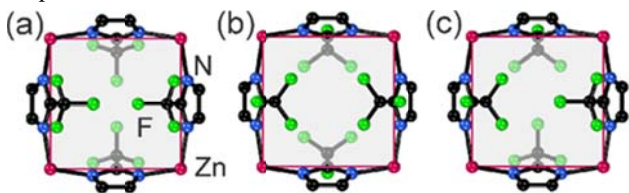


Figure 2. Illustration of different relative orientations of $-\text{CF}_3$ groups across a 4-ring: (a) head-to-head; (b) tail-to-tail; (c) head-to-tail.

Structures were geometry-optimized using periodic plane wave DFT code CASTEP 16.11,⁴¹ using the PBE functional with Grimme D2 SEDC.⁴² The I-centered structures

(*zni*, SOD, ANA, RHO) were transformed to corresponding primitive structures, reducing the cell volume and computational cost, while preserving all symmetry operations of the original structures. Optimized structures were also used for single point calculations with many-body dispersion (PBE+MBD*)⁴³⁻⁴⁵ energy model. While the Grimme D2 scheme relies on a parameterization of pairwise atom-atom interactions to compute dispersion energies, MBD* approach computes the interaction parameters from the energy density of a structure while including the many-body terms beyond the pairwise interaction. The plane wave basis set was truncated at 750 eV cutoff, and norm-conserving pseudopotentials were used for the core regions of electron density. The Brillouin zone was sampled with a 0.03 \AA^{-1} Monkhorst-Pack k-point grid.⁴⁶ Each structure was geometry optimized to an energy minimum with respect to unit cell dimensions and atom coordinates, subject to space group constraints. One exception to this protocol was the computationally-expensive RHO- $\text{Zn}(\text{CF}_3\text{Im})_2$ in $P1$ space group, generated from the optimized $Im\text{-}3m$ structure. Due to high computational cost, only the positions of atoms in $-\text{CF}_3$ groups were optimized, keeping the remaining atoms and unit cell parameters fixed. The applied strategy provided putative structures without any unusually short F...F contacts (see Table 1).

The electronic density of states (DOS) were calculated for the optimized ZIF structures, in order to assess any potential relationships between topological connectivity and electronic properties of $\text{Zn}(\text{CF}_3\text{Im})_2$ polymorphs. The DOS plots were calculated using the code OptaDOS.⁴⁷⁻⁴⁸ Further computational details are provided in the SI.

Experimental Methods

The experimentally determined structures for *qtz*- and $\text{SOD-Zn}(\text{CF}_3\text{Im})_2$ frameworks, as well as for the ligand HCF_3Im have been provided in the SI, in CIF format, and have also been deposited with the Cambridge Crystallographic Data Centre (CCDC codes 1859151-1859153).

Details of all experimental techniques, sample analysis, as well as examples of individual mechanochemical experiments are provided in the SI. In a typical mechanochemical experiment, reaction components were placed in a stainless steel jar of 10 mL volume, along with a milling liquid (50 μL per 0.1 mmol of each reactant, which maintained the liquid-to-solid ratio η ⁴⁹ below 0.25 $\mu\text{L}/\text{mg}$) and two stainless steel balls of 7 mm diameter (1.34 g weight each), mounted on a Retsch MM400 mill. The mill was operated at 30 Hz in all cases. All samples of metal-organic frameworks were washed three times with methanol (MeOH) and dried under vacuum at room temperature. The samples were all analyzed using powder X-ray diffraction (PXRD) and Fourier-transform infrared attenuated total reflectance (FTIR-ATR) spectroscopy. Selected samples were also analyzed using thermogravimetric analysis (TGA) and nitrogen sorption at 77K (see SI). The crystal structure of the ligand HCF_3Im was also determined using single crystal X-ray diffraction (see SI).

Dissolution enthalpies of $\text{Zn}(\text{CF}_3\text{Im})_2$ frameworks were measured with a CSC 4400 isothermal microcalorimeter operating at 25°C. A pellet (3-5 mg) of each chemical used in the thermodynamic cycle (see SI) was hand-pressed, weighed using a Mettler microbalance, and dropped into 25.0 g of isothermally equilibrated 5 M HCl aqueous solution inside a 50 mL Teflon cell of the calorimeter. After each experiment the cell was reassembled with fresh solvent. The sample was allowed to dissolve in the cell for at least 3 hours under mechanical stirring at approximately 1/2 Hz in all experiments. We have used a similar methodology in our previous thermochemical ZIF studies.^{20,50} The measured solution enthalpies and the calculated enthalpies of formation are summarized in the SI.

Results and discussion

Results of computational screening

Both SEDC approaches gave identical ranking of putative $\text{Zn}(\text{CF}_3\text{Im})_2$ frameworks (Table 1), which is consistent with our previous comparative study²⁸ of different SEDC schemes in calculating MOF stability. Both MBD*- and D2-based calculations indicate that the most stable form of $\text{Zn}(\text{CF}_3\text{Im})_2$ should be a non-porous *qtz*-framework. Experimental studies on $\text{Zn}(\text{MeIm})_2$ and $\text{Zn}(\text{EtIm})_2$ polymorphs, as well as other systems, indicate that open structures with calculated energy ($E_{\text{rel,c}}$) up to ~25-30 kJ mol⁻¹ above the lowest-energy one might be observable.^{20,51} Therefore, it is reasonable to assume that *qtz*-, *dia*- and *SOD*- $\text{Zn}(\text{CF}_3\text{Im})_2$, with calculated energies under 20 kJ mol⁻¹, could be experimentally accessible. While $E_{\text{rel,c}}$ for *kat*- $\text{Zn}(\text{CF}_3\text{Im})_2$ is just under 30 kJ mol⁻¹, this phase might be difficult to observe as it is a high-energy densely-packed structure (packing coefficient PC=0.70) that cannot be stabilized by guest inclusion.

Table 1 Topologies, calculated relative energies ($E_{\text{rel,c}}$, kJ mol⁻¹), volumes per formula unit (V, Å³), packing coefficients (PC) and shortest F...F distance ($d_{\text{F...F}}$, Å) for putative $\text{Zn}(\text{CF}_3\text{Im})_2$ polymorphs.

Topology	Space group	$E_{\text{rel,c}}$		V	PC	$d_{\text{F...F}}$
		PBE+D2	PBE+MBD*			
<i>qtz</i>	$P6_4$	0.00	0.00	270.5	0.66	3.06 ^c
<i>dia</i>	$P2_1/c^a$	11.29	13.49	265.9	0.74	2.74
<i>SOD</i> ^a	$P1^a$	19.01	15.93	436.4	0.45	2.89 ^d
	$I-43m$	25.17	20.90	442.0	0.44	3.49 ^d
<i>kat</i>	$P1^a$	26.20	27.02	280.4	0.70	2.63
	$P-42c$	35.59	36.84	282.7	0.69	2.54
<i>RHO</i>	$Im-3m$	34.60	33.47	534.6	0.36	2.53
	$P1^a$	34.75	34.14	534.6	0.36	2.53
<i>ANA</i>	$I-3ad$	43.87	45.25	409.0	0.47	2.87
	$P1^a$	44.31	45.24	408.7	0.47	2.75
<i>cag</i> ^b	$Pbca$	121.81	116.99	409.0	0.49	2.58
<i>zni</i> ^b	$I4_1cd$	182.15	181.58	296.1	0.65	2.41

^a-CF₃ groups across a 4-ring were placed in a “head-to-tail” orientation; ^boptimization was not successful, leading to

structure disruption; ^cthe shortest F...F distance in the subsequently established experimental structure is 3.08 Å; ^dthe shortest F...F distance in the subsequently established disordered experimental structure is 3.75 Å.

Calculations reveal a striking effect of -CF₃ group orientation on ZIF stability: switching from the ordered *P-42c* structure for *kat*- $\text{Zn}(\text{CF}_3\text{Im})_2$, in which -CF₃ groups are arranged “head-to-head” (Figure 2a), to the *P1* model with -CF₃ groups in the “head-to-tail” orientation (Figure 2c) produced an energy gain of ~10 kJ mol⁻¹ using either PBE+D2 or PBE+MBD* method. Corresponding difference for the less dense *SOD*- $\text{Zn}(\text{CF}_3\text{Im})_2$ was between 5.0 and 6.2 kJ mol⁻¹, and under 1 kJ mol⁻¹ for low-density *ANA*- and *RHO*- $\text{Zn}(\text{CF}_3\text{Im})_2$. These results show that orientation and potential disorder of -CF₃ groups can be an important factor in ZIF stability. Attempts to optimize *zni*- and *cag*- $\text{Zn}(\text{CF}_3\text{Im})_2$, based on topologies found in ZIFs containing the unsubstituted imidazolate linker, were unsuccessful. Modelling led to significant, unrealistic distortions, involving rupture of Zn-N bonds and formation of Zn-F bonds involving -CF₃ groups. This suggests that a -CF₃ group cannot be easily accommodated within structural models based on unsubstituted imidazole ligand.

In order to investigate the effects of crystal packing on the electronic properties of $\text{Zn}(\text{CF}_3\text{Im})_2$, electronic density of states (DOS) was calculated for all predicted structures. Despite the differences in lattice energy and packing density, all structures displayed remarkable similarity in their DOS plots and calculated band gaps (see SI). It is evident that the electron distribution in ZIFs mostly depends on the nature of nodes and ligands, rather than their network topology.

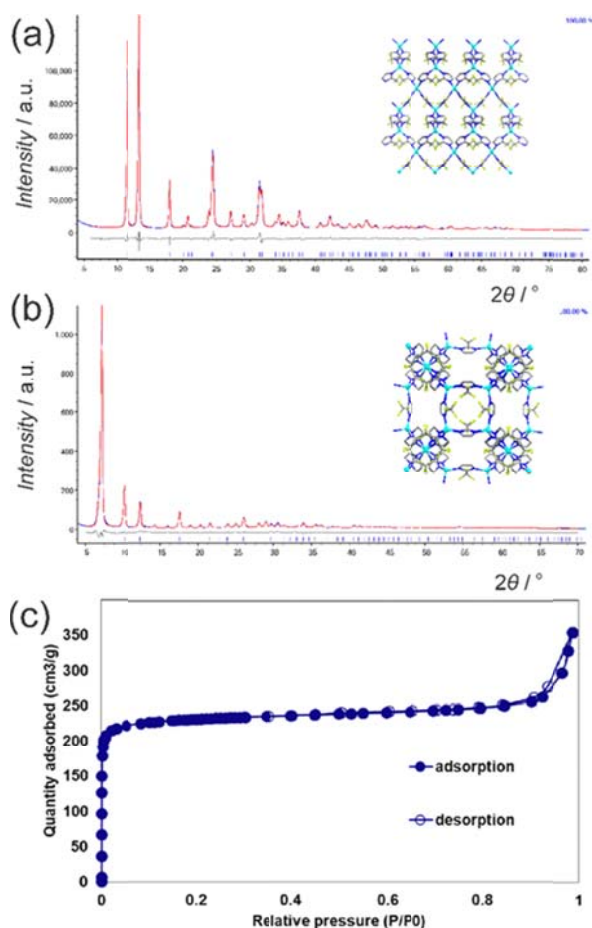


Figure 3. Final Rietveld refinement fits for: (a) qtz - $Zn(CF_3Im)_2$ and (b) SOD - $Zn(CF_3Im)_2$. (c) Nitrogen sorption isotherm measured at 77K for SOD - $Zn(CF_3Im)_2$.

Results of mechanochemical synthesis

Previous attempts to synthesize $Zn(CF_3Im)_2$ from solution were reported to be unsuccessful, instead leading to precipitation of ZnO and/or formation of oxo-bridged coordination polymers.³⁸ We based our synthesis on mechanochemical ion- and liquid-assisted grinding (ILAG),⁵² *i.e.* ball milling of stoichiometric amounts of ZnO and HCF_3Im (see SI) in presence of a liquid additive and a catalytic amount of a protic salt (NH_4NO_3 , 10 mol% relative to ZnO). Powder X-ray diffraction analysis of reaction mixtures after 20 minutes milling revealed different phases depending on choice of liquid: $CHCl_3$, methanol, N,N -dimethylformamide (DMF) and 1,1,1-trifluoroethanol (TFE) gave a new crystalline phase with characteristic Bragg reflections at 2θ of 11.5° and 13.5° . The PXRD pattern of the product obtained with DMF did not exhibit any reflections of reactants, indicating complete conversion, and on visual inspection was an excellent match to the computationally generated qtz - $Zn(CF_3Im)_2$ Structure and composition of qtz - $Zn(CF_3Im)_2$ were confirmed by Rietveld refinement (Figure 3a) and TGA in air (see SI for detailed experimental data).

In contrast, ILAG with ethanol or dioxane gave a product whose PXRD pattern was consistent with a mixture of

qtz - $Zn(CF_3Im)_2$ and a material isostructural to the putative SOD - $Zn(CF_3Im)_2$ phase. This phase was also observed for ILAG with $CHCl_3$, DMF, and TFE if milling was conducted for only 10 minutes (see SI), indicating that mechanochemical reaction of ZnO and HCF_3Im proceeds over two stages, yielding first the open SOD - $Zn(CF_3Im)_2$, followed by the close-packed qtz - $Zn(CF_3Im)_2$. Transformation to the qtz -polymorph made the synthesis of phase-pure SOD - $Zn(CF_3Im)_2$ challenging and, subsequently, a reliable synthesis was accomplished by milder liquid-assisted grinding (LAG)^{49,53} of the more reactive⁵⁴ basic zinc carbonate $[ZnCO_3]_2[Zn(OH)_2]_3$ in presence of ethanol. After methanol washing and evacuation, composition of SOD - $Zn(CF_3Im)_2$ was confirmed by TGA and Rietveld refinement (Figure 3b). Nitrogen sorption at 77K revealed a surface area of $923\text{ m}^2/\text{g}$, in good agreement with the value calculated from the crystal structure ($1017\text{ m}^2\text{ g}^{-1}$, Figure 3c, also see SI). The qtz - $Zn(CF_3Im)_2$ phase was non-porous, with measured surface area of $29\text{ m}^2\text{ g}^{-1}$.

Results of thermochemical measurements

Availability of phase-pure samples allowed us to evaluate enthalpies of formation (ΔH_f , Equation 1 in Figure 1b, Table 2) of qtz - and SOD - $Zn(CF_3Im)_2$ from ZnO and HCF_3Im , using dissolution enthalpies (ΔH_{ds} , Table 2) obtained by acid solution calorimetry (see SI).^{20,50,51}

Table 2 Dissolution (ΔH_{ds}), formation (ΔH_f) and transition (ΔH_{trans}) enthalpies for qtz - $Zn(CF_3Im)_2$, SOD - $Zn(CF_3Im)_2$ and related reaction components (kJ mol^{-1}).

Compound	ΔH_{ds}	ΔH_f	ΔH_{trans}
ZnO	-72.29 ± 0.17^a	-	-
HCF_3Im	-0.82 ± 0.03	-	-
H_2O	-0.5^a	-	-
qtz - $Zn(CF_3Im)_2$	-53.97 ± 0.20	-19.45 ± 0.27	27.25 ± 1.04
SOD - $Zn(CF_3Im)_2$	-69.61 ± 0.54	-3.82 ± 0.57	42.88 ± 1.15

^areferences 20, 55

All measured ΔH_f are exothermic, indicating that the formation of both frameworks from ZnO is thermodynamically driven. However, ΔH_f for SOD - $Zn(CF_3Im)_2$ is very small, which provides a tentative explanation for the formation of ZnO in attempts to obtain this material from solution.³⁸ The difference in ΔH_f for SOD - and qtz - $Zn(CF_3Im)_2$ is 15.63 kJ mol^{-1} , suggesting that the observed two-step mechanosynthesis mechanism, in which the initially formed SOD -phase transforms to qtz - $Zn(CF_3Im)_2$, follows Ostwald's rule of stages.⁵⁶

The ΔH_f difference between SOD - and qtz -polymorphs of $Zn(CF_3Im)_2$ is remarkably close to the $E_{rel,c}$ for SOD - $Zn(CF_3Im)_2$ obtained using the MBD* method (15.93 kJ mol^{-1} , Table 1), and is only 3.4 kJ mol^{-1} different from that obtained using D2. Such excellent agreement validates the use of SEDC, and particularly MBD* method, in calculating ZIF stability. This led us to revisit stabilities of $Zn(MeIm)_2$ polymorphs using PBE+MBD*, revealing excellent agreement with experiment (Table 3).²⁰

Table 3 Relative stabilities calculated using PBE+D2^a and PBE+MBD* methods ($E_{\text{rel,c}}$ kJ mol⁻¹) and experimental ΔH_{rel} (kJ mol⁻¹) for Zn(MeIm)₂ polymorphs.

Framework	$E_{\text{rel,c}}$ (PBE+D2) ^a	$E_{\text{rel,c}}$ (PBE+MBD*)	ΔH_{rel}
<i>dia</i> -Zn(MeIm) ₂	0.0	0.0	0.0
<i>kat</i> -Zn(MeIm) ₂	7.1	4.7	2.3
SOD-Zn(MeIm) ₂	15.2	11.2	10.6

^afrom reference 20.

The ΔH_f values were used to obtain a new set of energies, by subtracting the enthalpic effects related to water formation and the change in metal coordination environment, previously evaluated as -46.7 ± 1.0 kJ mol⁻¹.^{20,51,57,58} These transition enthalpies (ΔH_{trans} , Table 2) are a measure of enthalpic changes associated with pore formation and change in intermolecular interactions. The ΔH_{trans} for *qtz*- and SOD-Zn(CF₃Im)₂ are positive, indicating that the change in metal coordination environment is the principal reason for ZIF formation from ZnO. The comparison of ΔH_{trans} for SOD- and *qtz*-Zn(CF₃Im)₂ to those previously reported²⁰ for polymorphs of Zn(MeIm)₂ and Zn(EtIm)₂ reveals an unexpected effect of peripheral ligand and substituent on ZIF stability (Figure 4). Namely, switching between -CH₃, -C₂H₅ and -CF₃ substituents yields sets of ZIFs of similar network density (number of nodes per nm³) but with significant energy differences. For example, the network densities of SOD-Zn(CF₃Im)₂, SOD-Zn(MeIm)₂ and ANA-Zn(EtIm)₂ are close, but the frameworks span an energetic stability range of experimentally measured enthalpies of 28.4 kJ mol⁻¹. Similarly, *qtz*-Zn(CF₃Im)₂, *dia*-Zn(MeIm)₂ and *qtz*-Zn(EtIm)₂ have similar network densities, but with measured enthalpies over a range of 22.8 kJ mol⁻¹. In both sets of materials, the framework stability falls in the sequence -CF₃ < -CH₃ < C₂H₅. A similar effect is observed for pairs of ZIFs with identical topologies, e.g. SOD-Zn(CF₃Im)₂ vs SOD-Zn(MeIm)₂ and *qtz*-Zn(CF₃Im)₂ vs *qtz*-Zn(EtIm)₂. In both pairs the -CF₃ substituent produces a material with ca. 20 kJ mol⁻¹ more endothermic ΔH_f and ΔH_{trans} compared to the hydrocarbon one.

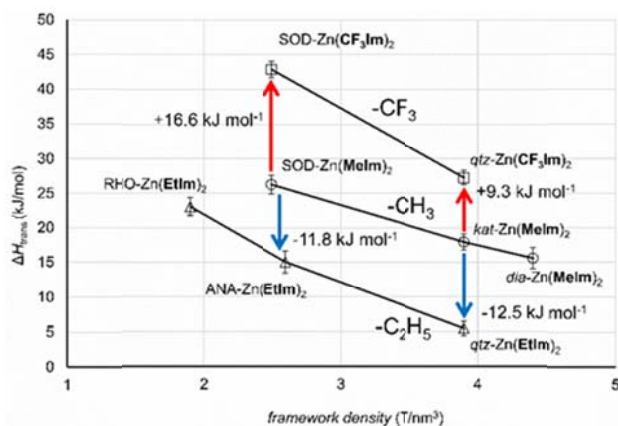


Figure 4. ΔH_{trans} for polymorphs of Zn(CF₃Im)₂, Zn(MeIm)₂,²⁰ and Zn(EtIm)₂,²⁰ highlighting energy differences between structures of similar framework density.

This is a remarkable result which indicates that hydrocarbon groups can notably increase the stability of a ZIF, while a fluorine-bearing substituent leads to destabilization. The presented results suggest a means to at least partially decouple the substituent effects on framework stability from its topology or network density. Qualitatively, this can be rationalized by changes in Zn-N bond strength, repulsion between -CF₃ substituents, and ability of hydrocarbon groups to form C-H... π interactions to adjacent imidazolate linkers.

Conclusions

In summary, this combined synthetic, theoretical and calorimetric study demonstrates the ability of dispersion-corrected periodic DFT to correctly model and anticipate the topological preferences for a previously not synthesized ZIF. Comparison of computational and thermochemical data shows that MBD* correction within periodic DFT CASTEP calculations also offers high accuracy in determining relative stabilities of ZIFs polymorphs, within 0.3-2.6 kJ mol⁻¹ from experiment. This study also reveals a surprising difference in stability between ZIFs exhibiting similar network density, but different choice of linker substituents, suggesting a potential route to manipulate thermodynamic stability of MOFs. While the calculations suggest that a *dia*-Zn(CF₃Im)₂ phase should also be accessible, the inability to observe it could be related to experimental limitations, similar to *kat*-Zn(MeIm)₂ which was observed years after SOD- and *dia*-forms. In that context, it is important to highlight the efficiency of mechanochemistry, which rapidly produced two polymorphs of previously not accessible³⁸ Zn(CF₃Im)₂. Overall, the herein demonstrated match between theory and experimental results is excellent and stands as a further benchmark for the modelling community — where the direct evaluation through experimental calorimetry remains rare.

ASSOCIATED CONTENT

Supporting information is available free of charge on the ACS Publications website (<http://pubs.acs.org>): additional experimental details and crystal structure descriptions, selected powder X-ray diffraction, thermal analysis, nitrogen sorption and infrared spectroscopy data, data for theoretically generated Zn(CF₃Im)₂ structures in CIF format, and data for experimentally determined crystal structures of HCF₃Im, *qtz*- and SOD-Zn(CF₃Im) in CIF format. The crystallographic data for experimental structures of HCF₃Im, *qtz*- and SOD-Zn(CF₃Im) has also been deposited with the Cambridge Crystallographic Data Centre (CCDC codes 1859151-1859153).

AUTHOR INFORMATION

Corresponding Authors

E-mails: tomlislav.frisic@mccgill.ca, anavrotsky@ucdavis.edu

Author Contributions

†These authors contributed equally

Funding Sources

This research is supported by the NSERC Discovery Grant (RGPIN-2017-06467), NSERC E. W. R. Steacie Memorial Fellowship (SMFSU 507347-17), U.S. Department of Energy Office of Science, grant DE-SC0016573.

Notes

The authors declare no competing financial interests.

ACKNOWLEDGMENT

We acknowledge support from the UK national high-performance computing service, ARCHER, for which access was obtained via the UKCP consortium and funded by EPSRC grant ref EP/P022561/1, and the use of the supercomputer Mp2 from University of Sherbrooke, managed by Calcul Québec and Compute Canada. The operation of this supercomputer is funded by the Canada Foundation for Innovation (CFI), the ministère de l'Économie, de la science et de l'innovation du Québec (MESI) and the Fonds de recherche du Québec - Nature et technologies (FRQ-NT).

REFERENCES

- (1) Farha, O. K.; Hupp, J. T. Rational Design, Synthesis, Purification, and Activation of Metal–Organic Framework Materials. *Acc. Chem. Res.* **2010**, *43*, 1166–1175.
- (2) Furukawa, H.; Cordova, K. E.; O’Keeffe, M.; Yaghi, O. M. The Chemistry and Applications of Metal–Organic Frameworks. *Science* **2013**, *341*, 1230444–1230444.
- (3) Rungtaweivoranit, B.; Diercks, C. S.; Kalmutzki, M. J.; Yaghi, O. M. Spiers Memorial Lecture: Progress and Prospects of Reticular Chemistry. *Faraday Discuss.* **2017**, *201*, 9–45.
- (4) Coudert, F.-X.; Fuchs, A. H. Computational Characterization and Prediction of Metal–organic Framework Properties. *Coord. Chem. Rev.* **2016**, *307*, 211–236.
- (5) Wilmer, C. E.; Leaf, M.; Lee, C. Y.; Farha, O. K.; Hauser, B. G.; Hupp, J. T.; Snurr, R. Q. Large-Scale Screening of Hypothetical Metal–organic Frameworks. *Nat. Chem.* **2012**, *4*, 83–89.
- (6) Chung, Y. G.; Gómez-Gualdrón, D. A.; Li, P.; Leperi, K. T.; Deria, P.; Zhang, H.; Vermeulen, N. A.; Stoddart, J. F.; You, F.; Hupp, J. T.; Farha, O. K.; Snurr, R. Q. In Silico Discovery of Metal–Organic Frameworks for Precombustion CO₂ Capture Using a Genetic Algorithm. *Sci. Adv.* **2016**, *2*, e1600909.
- (7) Witman, M.; Ling, S.; Anderson, S.; Tong, L.; Stylianou, K. C.; Slater, B.; Smit, B.; Haranczyk, M. In Silico Design and Screening of Hypothetical MOF-74 Analogs and Their Experimental Synthesis. *Chem. Sci.* **2016**, *7*, 6263–6272.
- (8) Moghadam, P. Z.; Islamoglu, T.; Goswami, S.; Exley, J.; Fantham, M.; Kaminski, C. F.; Snurr, R. Q.; Farha, O. K.; Fairen-Jimenez, D. Computer-Aided Discovery of a Metal–organic Framework with Superior Oxygen Uptake. *Nat. Commun.* **2018**, *9*, 1378.
- (9) Witman, M.; Ling, S.; Gladysiak, A.; Stylianou, K. C.; Smit, B.; Slater, B.; Haranczyk, M. Rational Design of a Low-Cost, High-Performance Metal–Organic Framework for Hydrogen Storage and Carbon Capture. *J. Phys. Chem. C* **2017**, *121*, 1171–1181.
- (10) Borboudakis, G.; Stergiannakos, T.; Frysali, M.; Klontzas, E.; Tsamardinos, I.; Froudakis, G. E. Chemically Intuited, Large-Scale Screening of MOFs by Machine Learning Techniques. *npj Comput. Mater.* **2017**, *3*, 40.
- (11) Collins, S. P.; Daff, T. D.; Piotrkowski, S. S.; Woo, T. K. Materials Design by Evolutionary Optimization of Functional Groups in Metal–Organic Frameworks. *Sci. Adv.* **2016**, *2*, e1600954.
- (12) Mellot-Draznieks, C.; Kerkeni, B. Exploring the Interplay between Ligand and Topology in Zeolitic Imidazolate Frameworks with Computational Chemistry. *Mol. Simul.* **2014**, *40*, 25–32.
- (13) Galvelis, R.; Slater, B.; Chaudret, R.; Creton, B.; Nieto-Draghi, C.; Mellot-Draznieks, C. Impact of Functionalized Linkers on the Energy Landscape of ZIFs. *CrystEngComm* **2013**, *15*, 9603–9612.
- (14) Baburin, I. A.; Leoni, S. The Energy Landscapes of Zeolitic Imidazolate Frameworks (ZIFs): Towards Quantifying the Presence of Substituents on the Imidazole Ring. *J. Mater. Chem.* **2012**, *22*, 10152–10154.
- (15) Liu, W.-G.; Truhlar, D. G. Computational Linker Design for Highly Crystalline Metal–Organic Framework NU-1000. *Chem. Mater.* **2017**, *29*, 8073–8081.
- (16) Zhang, J.-P.; Zhang, Y.-B.; Lin, J.-B.; Chen, X.-M. Metal Azolate Frameworks: From Crystal Engineering to Functional Materials. *Chem. Rev.* **2012**, *112*, 1001–1033.
- (17) Park, K. S.; Ni, Z.; Cote, A. P.; Choi, J. Y.; Huang, R.; Uribe-Romo, F. J.; Chae, H. K.; O’Keeffe, M.; Yaghi, O. M. Exceptional Chemical and Thermal Stability of Zeolitic Imidazolate Frameworks. *Proc. Natl. Acad. Sci.* **2006**, *103*, 10186–10191.
- (18) Huang, X. C.; Lin, Y. Y.; Zhang, J. P.; Chen, X. M. Ligand-Directed Strategy for Zeolite-Type Metal–Organic Frameworks: Zinc(II) Imidazolates with Unusual Zeolitic Topologies. *Angew. Chem. Int. Ed.* **2006**, *45*, 1557–1559.
- (19) He, C.-T.; Jiang, L.; Ye, Z.-M.; Krishna, R.; Zhong, Z.-S.; Liao, P.-Q.; Xu, J.; Ouyang, G.; Zhang, J.-P.; Chen, X.-M. Exceptional Hydrophobicity of a Large-Pore Metal–Organic Zeolite. *J. Am. Chem. Soc.* **2015**, *137*, 7217–7223.
- (20) Akimbekov, Z.; Katsenis, A. D.; Nagabhushana, G. P.; Ayoub, G.; Arhangelskis, M.; Morris, A. J.; Friščić, T.; Navrotsky, A. Experimental and Theoretical Evaluation of the Stability of True MOF Polymorphs Explains Their Mechanochemical Interconversions. *J. Am. Chem. Soc.* **2017**, *139*, 7952–7957.
- (21) Schröder, C. A.; Baburin, I. A.; van Wüllen, L.; Wiebcke, M.; Leoni, S. Subtle Polymorphism of Zinc Imidazolate Frameworks: Temperature-Dependent Ground States in the Energy Landscape Revealed by Experiment and Theory. *CrystEngComm* **2013**, *15*, 4036–4040.
- (22) Baburin, I. A.; Leoni, S.; Seifert, G. Enumeration of Not-yet-Synthesized Zeolitic Zinc Imidazolate MOF Networks: A Topological and DFT Approach. *J. Phys. Chem. B* **2008**, *112*, 9437–9443.
- (23) Lewis, D. W.; Ruiz-Salvador, A. R.; Gómez, A.; Rodriguez-Albelo, L. M.; Coudert, F.-X.; Slater, B.; Cheetham, A. K.; Mellot-Draznieks, C. Zeolitic Imidazole Frameworks: Structural and Energetics Trends Compared with Their Zeolite Analogues. *CrystEngComm* **2009**, *11*, 2272–2276.
- (24) Galvelis, R.; Slater, B.; Cheetham, A. K.; Mellot-Draznieks, C. Comparison of the Relative Stability of Zinc and Lithium–Boron Zeolitic Imidazolate Frameworks. *CrystEngComm* **2012**, *14*, 374–378.
- (25) Schweinefuß, M. E.; Springer, S.; Baburin, I. A.; Hikov, T.; Huber, K.; Leoni, S.; Wiebcke, M. Zeolitic Imidazolate Framework-71 Nanocrystals and a Novel SOD-Type Polymorph: Solution Mediated Phase Transformations, Phase Selection via Coordination Modulation and a Density Functional Theory Derived Energy Landscape. *Dalton Trans.* **2014**, *43*, 3528–3536.
- (26) Nazarian, D.; Camp, J. S.; Chung, Y. G.; Snurr, R. Q.; Sholl, D. S. Large-Scale Refinement of Metal–Organic Framework Structures Using Density Functional Theory. *Chem. Mater.* **2017**, *29*, 2521–2528.
- (27) Rosen, A. S.; Notestein, J. M.; Snurr, R. Q. Identifying Promising Metal–organic Frameworks for Heterogeneous Catalysis via High-throughput Periodic Density Functional Theory. *J. Comput. Chem.* **2019**, DOI: 10.1002/jcc.25787.

- (28) Arhangel'skii, M.; Katsenis, A. D.; Morris, A. J.; Frišćić, T. Computational Evaluation of Metal Pentazolate Frameworks: Inorganic Analogues of Azolate Metal-organic Frameworks. *Chem. Sci.* **2018**, *9*, 3367–3375.
- (29) Zhang, D.-S.; Chang, Z.; Li, Y.-F.; Jiang, Z.-Y.; Xuan, Z.-H.; Zhang, Y.-H.; Li, J.-R.; Chen, Q.; Hu, T.-L.; Bu, X.-H. Fluorous Metal-Organic Frameworks with Enhanced Stability and High H₂/CO₂ Storage Capacities. *Sci. Rep.* **2013**, *3*, 3312.
- (30) Cadiou, A.; Belmabkhout, Y.; Adil, K.; Bhatt, P. M.; Pillai, R. S.; Shkurenko, A.; Martineau-corcus, C.; Maurin, G.; Eddaoudi, M. Hydrolytically Stable Fluorinated Metal-Organic Frameworks for Energy-Efficient Dehydration. *Science* **2017**, *356*, 731–735.
- (31) Noro, S.; Nakamura, T. Fluorine-Functionalized Metal-organic Frameworks and Porous Coordination Polymers. *NPG Asia Mater.* **2017**, *9*, e433.
- (32) Bhatt, P. M.; Belmabkhout, Y.; Cadiou, A.; Adil, K.; Shekhah, O.; Shkurenko, A.; Barbour, L. J.; Eddaoudi, M. A Fine-Tuned Fluorinated MOF Addresses the Needs for Trace CO₂ Removal and Air Capture Using Physisorption. *J. Am. Chem. Soc.* **2016**, *138*, 9301–9307.
- (33) Pachfule, P.; Chen, Y.; Jiang, J.; Banerjee, R. Fluorinated Metal-Organic Frameworks: Advantageous for Higher H₂ and CO₂ Adsorption or Not? *Chem. Eur. J.* **2012**, *18*, 688–694.
- (34) Chen, T.-H.; Popov, I.; Kaveevivitchai, W.; Chuang, Y.-C.; Chen, Y.-S.; Jacobson, A. J.; Miljanić, O. Š. Mesoporous Fluorinated Metal-Organic Frameworks with Exceptional Adsorption of Fluorocarbons and CFCs. *Angew. Chem. Int. Ed.* **2015**, *54*, 13902–13906.
- (35) Belmabkhout, Y.; Bhatt, P. M.; Adil, K.; Pillai, R. S.; Cadiou, A.; Shkurenko, A.; Maurin, G.; Liu, G.; Koros, W. J.; Eddaoudi, M. Natural Gas Upgrading Using a Fluorinated MOF with Tuned H₂S and CO₂ Adsorption Selectivity. *Nat. Energy* **2018**, *3*, 1059–1066.
- (36) Liu, G.; Cadiou, A.; Liu, Y.; Adil, K.; Chernikova, V.; Carja, I. D.; Belmabkhout, Y.; Karunakaran, M.; Shekhah, O.; Zhang, C.; Itta, A. K.; Yi, S.; Eddaoudi, M.; Koros, W. J. Enabling Fluorinated MOF-Based Membranes for Simultaneous Removal of H₂S and CO₂ from Natural Gas. *Angew. Chem. Int. Ed.* **2018**, *57*, 14811–14816.
- (37) Tchalala, M. R.; Belmabkhout, Y.; Adil, K.; Chappanda, K. N.; Cadiou, A.; Bhatt, P. M.; Salama, K. N.; Eddaoudi, M. Concurrent Sensing of CO₂ and H₂O from Air Using Ultramicroporous Fluorinated Metal-Organic Frameworks: Effect of Transduction Mechanism on the Sensing Performance. *ACS Appl. Mater. Interfaces* **2019**, *11*, 1706–1712.
- (38) Mondal, S. S.; Hovestadt, M.; Dey, S.; Paula, C.; Glomb, S.; Kelling, A.; Schilde, U.; Janiak, C.; Hartmann, M.; Holdt, H.-J. Synthesis of a Partially Fluorinated ZIF-8 Analog for Ethane/Ethene Separation. *CrystEngComm* **2017**, *19*, 5882–5891.
- (39) Katsenis, A. D.; Puškarić, A.; Štrukil, V.; Mottillo, C.; Julien, P. A.; Užarević, K.; Pham, M.-H.; Do, T.-O.; Kimber, S. A. J.; Lazić, P.; Magdysyuk, O.; Dinnebier, R. E.; Halasz, I.; Frišćić, T. In Situ X-Ray Diffraction Monitoring of a Mechanochemical Reaction Reveals a Unique Topology Metal-Organic Framework. *Nat. Commun.* **2015**, *6*, 6662.
- (40) Cambridge Structural Database (CSD), version 5.39 (February 2018).
- (41) Clark, S. J.; Segall, M. D.; Pickard, C. J.; Hasnip, P. J.; Probert, M. I. J.; Refson, K.; Payne, M. C. First Principles Methods Using CASTEP. *Z. Kristallogr.* **2005**, *220*, 567–570.
- (42) Grimme, S. Semiempirical GGA-Type Density Functional Constructed with a Long-Range Dispersion Correction. *J. Comput. Chem.* **2006**, *27*, 1787–1799.
- (43) Tkatchenko, A.; DiStasio Jr, R. A.; Car, R.; Scheffler, M. Accurate and Efficient Method for Many-Body van Der Waals Interactions. *Phys. Rev. Lett.* **2012**, *108*, 236402.
- (44) Ambrosetti, A.; Reilly, A. M.; DiStasio, R. A.; Tkatchenko, A. Long-Range Correlation Energy Calculated from Coupled Atomic Response Functions. *J. Chem. Phys.* **2014**, *140*, 18A508.
- (45) Reilly, A. M.; Tkatchenko, A. Van Der Waals Dispersion Interactions in Molecular Materials: Beyond Pairwise Additivity. *Chem. Sci.* **2015**, *6*, 3289–3301.
- (46) Monkhorst, H. J.; Pack, J. D. Special Points for Brillouin-Zone Integrations. *Phys. Rev. B* **1976**, *13*, 5188–5192.
- (47) Nicholls, R. J.; Morris, A. J.; Pickard, C. J.; Yates, J. R. OptaDOS - a New Tool for EELS Calculations. *J. Phys. Conf. Ser.* **2012**, *371*, 012062.
- (48) Morris, A. J.; Nicholls, R. J.; Pickard, C. J.; Yates, J. R. OptaDOS: A Tool for Obtaining Density of States, Core-Level and Optical Spectra from Electronic Structure Codes. *Comput. Phys. Commun.* **2014**, *185*, 1477–1485.
- (49) Frišćić, T.; Childs, S. L.; Rizvi, S. A. A.; Jones, W. The Role of Solvent in Mechanochemical and Sonochemical Cocystal Formation: A Solubility-Based Approach for Predicting Crystallisation Outcome. *CrystEngComm* **2009**, *11*, 418–426.
- (50) Hughes, J. T.; Bennett, T. D.; Cheetham, A. K.; Navrotsky, A. Thermochemistry of Zeolitic Imidazolate Frameworks of Varying Porosity. *J. Am. Chem. Soc.* **2013**, *135*, 598–601.
- (51) Akimbekov, Z.; Navrotsky, A. Little Thermodynamic Penalty for the Synthesis of Ultraporous Metal Organic Frameworks. *ChemPhysChem* **2016**, *17*, 468–470.
- (52) Do, J.-L.; Frišćić, T. Mechanochemistry: A Force of Synthesis. *ACS Cent. Sci.* **2017**, *3*, 13–19.
- (53) Frišćić, T. New Opportunities for Materials Synthesis Using Mechanochemistry. *J. Mater. Chem.* **2010**, *20*, 7599–7605.
- (54) Yuan, W.; Frišćić, T.; Apperley, D.; James, S. L. High Reactivity of Metal-Organic Frameworks under Grinding Conditions: Parallels with Organic Molecular Materials. *Angew. Chem. Int. Ed.* **2010**, *49*, 3916–3919.
- (55) Parker, V. B. *Thermal Properties of Aqueous Uni-Univalent Electrolytes*; Dept. of Commerce, National Bureau of Standards: Washington, D. C., 1965.
- (56) Burley, J. C.; Duer, M. J.; Stein, R. S.; Vrcelj, R. M. Enforcing Ostwald's Rule of Stages: Isolation of Paracetamol Forms III and II. *Eur. J. Pharm. Sci.* **2007**, *31*, 271–276.
- (57) Wu, D.; Navrotsky, A. Thermodynamics of Metal-Organic Frameworks. *J. Solid State Chem.* **2015**, *223*, 53–58.
- (58) Akimbekov, Z.; Wu, D.; Brozek, C. K.; Dincă, M.; Navrotsky, A. Thermodynamics of Solvent Interaction with the Metal-organic Framework MOF-5. *Phys. Chem. Chem. Phys.* **2016**, *18*, 1158–1162.

